



Full Length Article

Solubility and crystallisability of the ternary system: Hexadecane and octadecane representative in fuel solvents

Xue Tang^a, Peter L. Kaskiewicz^a, Diana M. Camacho Corzo^a, Xiaojun Lai^a, Kevin J. Roberts^{a,*}, Peter Dowding^b, Iain More^b^a School of Chemical and Process Engineering, University of Leeds, Leeds, UK^b Infineum UK Ltd, Milton Hill Business and Technology Centre, Abingdon, UK

ARTICLE INFO

Keywords:

Biofuel cold-flow behaviour
Alkane
Hexadecane
Octadecane
Ternary system
Solubility
Solvent effect
Solution thermodynamics
Saturation temperature
Metastable zone width
Crystallisability
Poly-thermal method
Turbidometric characterisation

ABSTRACT

The solubility and crystallisability of a range of binary mixtures of n-hexadecane (C₁₆H₃₄) and n-octadecane (C₁₈H₃₈), as the predominant alkanes present in hydrotreated vegetable oil (HVO), from three representative fuel solutions (dodecane, toluene and kerosene) is presented. The dissolution (saturation) and crystallisation (supersaturation) points of the solutions are measured using poly-thermal methods utilising turbidometric detection over four concentrations from (192 g/l to 400 g/l). The data reveals the existence of more soluble, less stable crystal structures that form from the alkane mixtures, when compared to the stable triclinic crystal structures formed from the single solute component solutions. An increased carbon chain length results in lower solubility for all three solvents and the solvent type is not found to have any significant effect on the solid forms produced from the mixtures. van't Hoff analysis reveals the solvent type to influence the solute solubility with the closest to ideal behaviour being dodecane followed by kerosene and toluene, respectively. This finding is further supported by the calculated dissolution enthalpies and activity coefficients, which are the lowest in dodecane followed by kerosene and toluene. Larger values of activity coefficients are observed for compositions with molar fraction (γ) = 0.1, 0.5–0.7 C₁₈H₃₈ which reflect the complex multi-phase formation in the solutions when compared with the more simple binary melt crystallisation system.

1. Introduction

A global concern towards greenhouse gas emissions and their impact on the environment has led to an ever-increasing use of sustainable, bio-derived feedstocks in fuel oils. By 2020, 10% of biofuel will be shared in transport as a blend component with the traditional fossil oil according to the target set by the European Union (EU) [1]. This second generation of biofuel has been intensively investigated by the EU due to its advantages regarding its compatibility with diesel fuel and its very high cetane number which can boost the fuel properties [2]. This biofuel can be produced by one- or more-step catalytic hydrotreating of different triglyceride containing vegetable oils (HVO) with typical production of a mixture of paraffins, namely C₁₅H₃₂, C₁₆H₃₄, C₁₇H₃₆ and C₁₈H₃₈ [3].

Technologically, the cold flow properties (notably its cloud and pour points) of hydrocarbon fuels, such as diesel and HVO are undesirable due to the high crystallisation temperatures of the long-chain alkanes within the fuel. The high molecular weight alkanes become

supersaturated during cooling, which results in the precipitation of less soluble flat plate-like wax crystals, which can aggregate together to form an impermeable mass that can melt together and block a vehicle's fuel filter, causing low operability of vehicles in cold climate regions. Conventional additives can inhibit nucleation and partly destabilise the fast-growing faces of these wax crystals and produce more compact habits in which the crystals are usually tabular in shape and reduced in size, respectively. However, the consequence of variance distribution of carbon number blending with 10% HVO³ into the traditional diesel [4] (Fig. 1) effects the carbon number chain distribution of the fuel fraction leading, in turn, to changes in the crystallisation behaviour and, potentially, the solid form that results. This outcome provides the incentive to obtain an improved fundamental knowledge of the crystallisation behaviour of blended HVO/diesel fuels in order to understand and mitigate any negative impact of HVO addition on the resulting cold flow properties of the fuel.

Since the studies of Müller [5–8], there has been much research into the crystalline structures of a wide range of alkanes (C_nH_{2n+2}). Full

Abbreviations: EU, European Union; HVO, Hydrotreated vegetable oil; KBHR, Kashchiev–Borissova–Hammond–Roberts; MSZW, Metastable zone width; PXRD, Powder X-ray diffraction; STD, Standard deviation; XRD, X-ray diffraction

* Corresponding author.

E-mail address: K.J.Roberts@leeds.ac.uk (K.J. Roberts).

<https://doi.org/10.1016/j.fuel.2018.04.022>

Received 25 January 2018; Received in revised form 29 March 2018; Accepted 4 April 2018

0016-2361/© 2018 The Authors. Published by Elsevier Ltd. This is an open access article under the CC BY license (<http://creativecommons.org/licenses/by/4.0/>).

List of symbols

C_nH_{2n+2}	alkane
$C_{16}H_{34}$	N-hexadecane
$C_{18}H_{38}$	N-octadecane
C_p	Heat capacity
M011	Monoclinic structure, space group (P2 ₁ /a)
M _{dci}	Monoclinic structure with conformational defects, space group (Aa)
n	Number
O _{dci}	Orthorhombic structure with conformation defects, space group (Pnam)
O _i	Orthorhombic structure, space group (Pcam)
O _p	Orthorhombic structure, space group (Pca2 ₁)
q	Cooling rate (°C/min)
R	Ideal gas constant (J/K.mol)
R _I	Rotator phase with orthorhombic structure, space group (Fmmm)
R _{II}	Rotator phase with orthorhombic structure, space group (R $\bar{3}$ m)
R _{III}	Rotator phase with triclinic structure

R _{IV}	Rotator phase with monoclinic structure
R _V	Rotator phase with monoclinic structure
T	Solution temperature (°C)
T _c	Crystallisation temperature (°C)
T _{c,l}	Crystallisation temperature at the kinetic limit/equilibrium crystallisation temperature (°C)
T _{diss}	Dissolution temperature (°C)
T _e	Equilibrium saturation temperature (°C)
T _p	Triclinic structure, space group (P $\bar{1}$)
x	Molar solubility
x_i deal	Molar solubility in ideal state
y	Mol fraction C ₁₈ H ₃₈ in C ₁₆ H ₃₄
a	Activity of the solid phase
a_s	Activity of the solute in solution
T _m	Melting point (°C)
ΔH_f	Enthalpy of fusion (kJ/mol)
ΔH_{diss}	Molar enthalpy of dissolution (kJ/mol)
ΔS_{diss}	Molar enthalpy of dissolution (kJ/K.mol)
ΔS_f	Entropy of fusion (kJ/K.mol)
γ	Activity coefficient

crystal-structure determination from single crystals of C₂₃H₄₈, C₃₆H₇₄ and C₁₈H₃₈, was carried out by Smith [9], Shearer [10], Nyburg and Luth [11], respectively. Further research relating towards lattice parameter measurements was performed by Retief [12,13], Nyburg and Potworowski [14], Luth [15] and Craig [16]. The latter confirmed the unit cell parameters as measured using high resolution synchrotron powder X-ray diffraction (PXRD), from C₁₃H₂₈ to C₆₀H₁₂₂ for even parity alkanes: triclinic (P $\bar{1}$) for [12 ≤ C_nH_{2n+2} ≤ 26] to monoclinic (P2₁/a) for [28 ≤ C_nH_{2n+2} ≤ 36] to orthorhombic (Pca2₁) for (C₃₆H₇₄, C₄₆H₉₄, C₅₀H₁₀₂ and C₆₀H₁₂₂). Odd parity alkanes were confirmed to have the Pbcm orthorhombic structure. It has also been found that disordered (rotator) phases are present between the liquid phase and the lower temperature ordered crystal phases, associated with rotational molecular positional disorder around the long molecular axis of the alkane molecules [17–20]. For even number alkanes, rotator phases were only observed in the longer chain systems with, C_nH_{2n+2} ≥ 20, with their stability being highly dependent on chain length [17,20]. The most common rotator phase has been found to be R_I structure, space group (Fmmm), which occurs in odd alkanes, C₁₁H₂₄ through C₂₅H₅₂,

and solid solution mixtures of even and odd alkanes within this range [18,19].

The known phase behaviour for binary mixtures in the range of C₈H₁₈–C₂₈H₅₈ was summarised by D. Mondieig et al. [21] for systems with Δn = 1 and 2. This revealed a number of additional phases by mixing – R_I at high temperature and the ordered phases of Odci, Mdcip, and Op forms at low temperature, shown in Table 1.

The solubility of alkanes has been widely studied, with a large amount of experimental data collected, regarding solutions containing either one or two solutes, which create pure crystals of the independent components [22–27]. However, studies of systems that form mixed crystals, i.e. solid solutions in a solvent environment, have been very limited, e.g. Gerson [28] and Flöter [29] who studied mixtures of C₂₀H₄₂–C₂₂H₄₆ in dodecane and n-heptane solutions, respectively. Both studies examined the saturation temperatures as a function of varying mixture composition, observing a clear pattern in saturation temperatures and the formation of different solid-solution phases. However, the phases of the solid solutions formed were not clearly defined in these studies. Early synchrotron diffraction work by Cunningham et al. [30] and Gerson et al. [31–33] suggested the existence of complex phase behaviour with triclinic, and up to three orthorhombic phases.

A recent PhD study [34] by one of the authors has provided some insight into phase behaviour understanding of C₁₆H₃₄–C₁₈H₃₈ binary mixtures and a subsequent ternary system in kerosene solutions. Examination of the binary C₁₆H₃₄–C₁₈H₃₈ equilibrium phase diagram

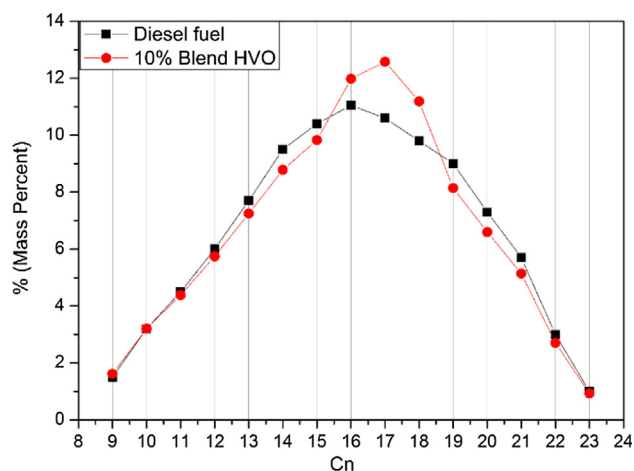


Fig. 1. Representative alkane distribution curves in traditional diesel fuel (■) and the blended fuel with 90% diesel + 10% HVO (●). This shows the variance distribution of carbon number blending with 10% HVO into the traditional diesel [3,4] highlighting an enhancement in the C₁₆H₃₄: C₁₈H₃₈ content.

Table 1

Crystallographic characteristics of pure alkanes [21]. Subscripts ‘dc’, ‘i’ and ‘p’ represent conformational defects, even parity and odd parity, respectively. M011 is one of the M(hkl) phases; where (hkl) describes the plane formed by the methyl end groups in the referential of the orthorhombic subcell.

Phase	C _n H _{2n+2} /C _n H _{2n+2} Range	Crystal System	Space Group	Z
R _I	9 ≤ n _{odd} ≤ 25 and n _{even} = 22,24	Orthorhombic		4
R _{II}	22 ≤ n ≤ 26	Trigonal		3
R _{III}	28	Triclinic	–	–
R _{IV}	28	Monoclinic	–	–
R _V	23, 25	Monoclinic	–	–
T _p	8 ≤ n _{even} ≤ 24	Triclinic		1
M011	n _{even} ≥ 26	Monoclinic		2
O _i	n _{odd}	Orthorhombic		4
O _{dci}	n _{odd} ≥ 23	Orthorhombic		4
M _{dci}	n _{odd} ≥ 25	Monoclinic		4
O _p	36	Orthorhombic		4

revealed that the R_1 phase was observed most for mixture compositions and stabilized at a wide temperature range. However, examination of the phase diagram for the tertiary system of $C_{16}H_{34}$: $C_{18}H_{38}$ in kerosene solution revealed a distinctly different phase behaviour, in which the R_1 phase was only observed over a small composition range and the more ordered phases of T_p ($P\bar{1}$) and O_p ($Pca2_1$) were found to be predominant.

In this paper the crystallisation behaviour with respect to solubility and crystallisability of mixtures of $C_{16}H_{34}$ and $C_{18}H_{38}$ as a model system of HVO blended fuels in solution environment is investigated with the associated solid form phase behaviour which is analysed with the help of previous X-ray studies [34]. Three solvents, aliphatic (dodecane), aromatic (toluene) and aliphatic-aromatic mixture (kerosene) were selected in order to gain an understanding of this behaviour when the mixed crystals are crystallised from solutions with components found in typical diesel fuel and to investigate the associated solution chemistry effects.

2. Materials and methods

2.1. Materials

Dodecane (99% pure), toluene ($\geq 99.3\%$ pure), $C_{16}H_{34}$ (99% pure) and $C_{18}H_{38}$ (99% pure) were supplied by Sigma-Aldrich. Kerosene (99% pure) was obtained from Infineum Ltd.; the composition, as determined by gas chromatography [35].

2.2. Experimental apparatus

Crystallisation experiments were performed using the Technobis Crystal 16® system [36]. This system comprises sixteen wells that are split into four blocks, consisting of four wells each. Each block is independently temperature-controlled to allow different temperature profiles to be set simultaneously with the use of Peltier elements and an external cooling device. Each well can hold a magnetically stirred 1 ml disposable glass vial. A laser beam passes through the vials in order to determine turbidity and provide information about the cloud and clear points of up to 16 solutions and turbidity data are recorded as a function of the temperature.

2.3. Experimental procedure

2.3.1. Solution preparation

All solutions were prepared at four solution concentrations for each solvent used, (192, 231, 269, 308 g/l), (300, 350, 400, 450 g/l), and (231, 269, 308, 350 g/l) for solvents of dodecane, toluene, and kerosene, respectively. For each solvent, eleven compositions of the $C_{16}H_{34}$: $C_{18}H_{38}$ binary mixtures in 10% molar increments were weighed using a weighing scale that could measure with ± 0.1 mg accuracy. Once the samples containing both $C_{16}H_{34}$ and $C_{18}H_{38}$ had been formed, the mixtures were placed in a shaker with an external temperature control system (F32 Julabo temperature bath), at 55 °C for 30 min in order for a melt to form. After this stage, a Fisherbrand 100–1000 μ l micropipette was used to add the respective solvent to each

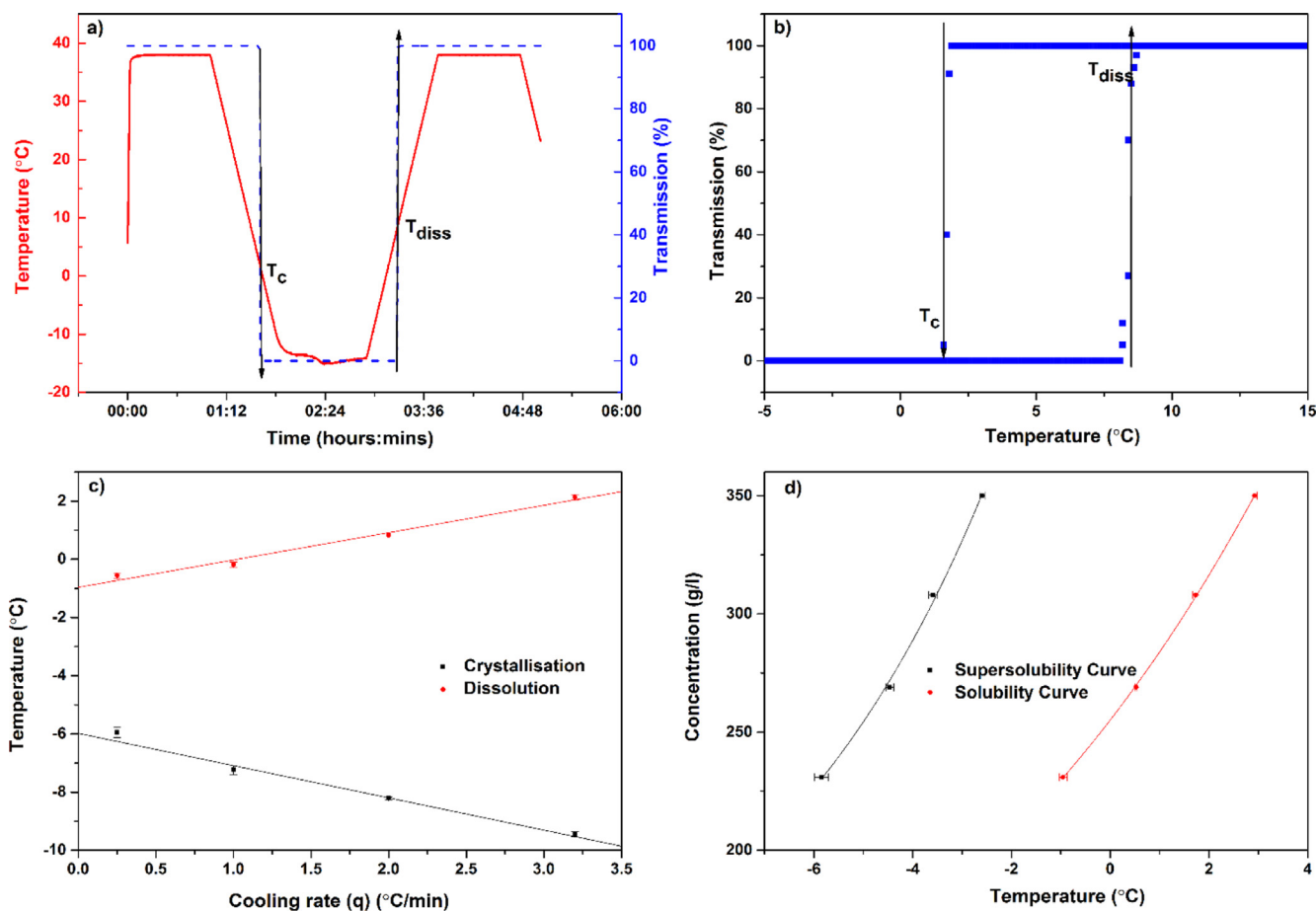


Fig. 2. Representative poly-thermal data: Temperature and transmission profiles against the time as used for measuring the crystallisation and dissolution for the solution; (b) Temperature turbidity plot of a solution highlighting the observation of on-set points for crystallisation (T_c) and (T_{diss}); (c) Plots of T_{diss} and T_c as a function of cooling rate (q) with the corresponding best linear fits are also given; (d) Concentration/temperature plot highlighting the MSZW between the solubility and supersolubility curves. (All data is for $y = 0.5$ of $C_{18}H_{38}$ in kerosene, where y is the mole fraction of the longer alkane $C_{18}H_{38}$ in $C_{16}H_{34}$).

concentration sample. The resulting mixtures were placed in the same shaker, at 55 °C for 30 min under a shaking rate of 150 rpm, in order to form a homogeneous liquid solution. The solutions were then filled into the 1 ml vials and a standard small magnetic stirrer was added to each vial.

2.3.2. Poly-thermal measurements and analysis

The 1 ml solutions were subject to different cooling and heating cycles. Each temperature cycle began by heating the solutions to 40 °C, before being held at this temperature for one hour to ensure that complete homogenisation had taken place and was then subsequently cooled at a set rate to –15 °C. This temperature was then held for an hour to allow equilibration, followed by an increase in temperature back to 40 °C at the specified rate. This temperature profile was performed for each concentration of each composition at rates (q) of 0.25, 1, 2 and 3.2 °C/min for both the cooling and heating segments of the temperature cycles with constant stirring at 300 rpm. Each temperature cycle was performed five times to obtain mean and standard deviation (STD) values for the crystallisation and dissolution temperatures.

The crystallisation (T_c) and dissolution temperatures (T_{diss}) were estimated based upon the turbidity profile, where sudden changes in light transmittance were detected. The values of transmittance ranged from 100%, for a homogeneous liquid solution, to 0%, for a fully crystallised solution. T_c was taken as the onset point where the light transmittance dropped approximately 10% from 100% and T_{diss} was taken as the point where the light transmittance reached 100% for all measurements. The poly-thermal data was used to extrapolate both $T_c(q)$ and $T_{diss}(q)$ lines back to a cooling rate of 0 °C/min so that the crystallisation temperatures at the kinetic limit ($T_{c,l}$) and equilibrium saturation temperatures (T_c) could be determined, respectively.

Table 2

Solubility (T_c) and supersolubility ($T_{c,l}$) data of $C_{16}H_{34}:C_{18}H_{38}$ mixtures in dodecane solvent, together with the calculated equilibrium MSZW (ΔT) over four concentrations (192–308 g/l). STD values from 5 recycles of repeats are also presented. y is the mole fraction of the longer alkane $C_{18}H_{38}$ in $C_{16}H_{34}$.

Con. (g/l)	$T_{c,l}$ (°C)	STD	T_c (°C)	STD	ΔT (°C)	STD	Con. (g/l)	$T_{c,l}$ (°C)	STD	T_c (°C)	STD	ΔT (°C)	STD
y = 0							y = 0.1						
192	–8.87	0.32	–4.49	0.11	4.37	0.58	192	–13.56	0.07	–7.87	0.11	5.68	0.16
231	–6.11	0.44	–2.80	0.15	3.32	0.47	231	–11.27	0.08	–5.40	0.11	5.87	0.14
269	–3.72	0.49	–1.02	0.34	2.70	0.04	269	–9.27	0.07	–4.11	0.09	5.16	0.12
308	–2.46	0.66	–0.03	0.10	2.43	0.29	308	–8.21	0.05	–3.00	0.08	5.21	0.09
y = 0.2							y = 0.3						
192	–13.04	0.06	–8.80	0.07	4.24	0.12	192	–11.82	0.07	–7.86	0.10	3.96	0.15
231	–10.61	0.07	–8.41	0.15	2.21	0.21	231	–9.50	0.08	–7.69	0.14	1.81	0.21
269	–9.11	0.07	–7.11	0.06	2.00	0.11	269	–7.63	0.11	–6.73	0.14	0.90	0.21
308	–7.42	0.08	–5.86	0.14	1.56	0.17	308	–6.34	0.04	–5.89	0.09	0.45	0.12
y = 0.4							y = 0.5						
192	–10.38	0.10	–5.05	0.05	5.33	0.12	192	–6.18	0.24	–1.71	0.11	4.47	0.15
231	–8.54	0.10	–3.14	0.06	5.41	0.16	231	–4.65	0.13	0.15	0.07	4.80	0.11
269	–6.63	0.06	–2.16	0.05	4.47	0.04	269	–3.35	0.19	1.73	0.09	5.08	0.27
308	–5.34	0.08	–0.73	0.11	4.61	0.14	308	–2.45	0.18	3.01	0.12	5.46	0.27
y = 0.6							y = 0.7						
192	–2.77	0.15	–0.54	0.03	2.23	0.18	192	–0.36	0.13	1.62	0.06	1.98	0.12
231	–1.55	0.20	1.65	0.08	3.21	0.25	231	0.88	0.30	3.39	0.16	2.51	0.25
269	0.00	0.05	3.13	0.13	3.12	0.14	269	2.75	0.24	5.05	0.07	2.30	0.27
308	1.30	0.12	4.10	0.02	2.81	0.12	308	3.67	0.16	6.57	0.08	2.90	0.15
y = 0.8							y = 0.9						
192	2.20	0.10	2.71	0.12	0.52	0.15	192	3.94	0.18	4.29	0.09	0.36	0.26
231	3.98	0.06	4.95	0.23	0.98	0.26	231	5.17	0.23	6.18	0.08	1.01	0.30
269	5.41	0.04	6.16	0.09	0.75	0.12	269	6.74	0.10	7.63	0.07	0.89	0.16
308	6.41	0.06	7.75	0.08	1.35	0.13	308	7.50	0.24	9.29	0.14	1.79	0.31
y = 1													
192	4.47	0.50	5.68	0.09	1.22	0.52							
231	6.53	0.46	7.42	0.19	0.88	0.59							
269	7.87	0.31	9.05	0.13	1.19	0.36							
308	9.47	0.02	10.17	0.15	0.70	0.13							

3. Results

Examples of poly-thermal heating-cooling and turbidity profiles used for the temperature cycles are displayed in Fig. 2(a) and (b), highlighting the determination of T_{diss} and T_c . The equilibrium solubility (T_e) and supersolubility ($T_{c,l}$) temperatures obtained from extrapolation of T_{diss} and T_c back to 0 °C/min are given in Tables 2–4 together with their MSZW for $C_{16}H_{34}:C_{18}H_{38}$ binary mixtures in solution of dodecane, toluene and kerosene, respectively. Examples of the linear regression plots of T_c and T_{diss} vs. q together with their STD values from five repeats and the resulting solubility-supersolubility curves are given in Fig. 2(c) and (d), respectively. The full list of T_{diss} and T_c together with calculated MSZW values for all cooling rates in dodecane, toluene and kerosene can be found in Tang et al. [35]. No literature data is available on the solubility in the ternary system studied. All the solutions measured in this study showed high repeatability from five repeats of cycling experiments with low standard deviation values.

4. Data analysis and discussion

4.1. Saturation temperature

The saturation temperatures (T_c) calculated for the model system of $C_{16}H_{34}:C_{18}H_{38}$ binary mixtures in the three solvents were used to form plots of T_c vs. molar composition. The resultant patterns in four concentrations of each solvent are quite consistent [35] and indicate that this effect is largely independent of concentration over the range studied. An example plot using dodecane and kerosene at 308 g/l and toluene at 350 g/l is shown in Fig. 3. The same trend of saturation temperature vs. composition over the three solvents suggests that structural behaviour is not dependent on the solvents used in this study. Under this condition the varying solubility is caused by compositional

Table 3

Solubility (T_e) and supersolubility ($T_{e,l}$) data of $C_{16}H_{34}$: $C_{18}H_{38}$ mixtures in toluene solvent, together with the calculated equilibrium MSZW (ΔT) over four concentrations (300–450 g/l). STD values from 5 recycles of repeats are also presented. y is the mole fraction of the longer alkane $C_{18}H_{38}$ in $C_{16}H_{34}$.

Con. (g/l)	$T_{e,l}$ (°C)	STD	T_e (°C)	STD	ΔT (°C)	STD	Con. (g/l)	$T_{e,l}$ (°C)	STD	T_e (°C)	STD	ΔT (°C)	STD
$y = 0$							$y = 0.1$						
300	-5.42	0.40	-4.20	0.15	1.22	0.53	300	-10.63	0.23	-7.56	0.12	3.07	0.31
350	-3.92	0.32	-2.71	0.11	1.22	0.40	350	-9.51	0.26	-6.44	0.42	3.07	0.46
400	-3.44	0.27	-2.04	0.35	1.39	0.26	400	-8.74	0.06	-5.16	0.20	3.59	0.20
450	-2.26	0.39	-1.09	0.11	1.17	0.39	450	-7.66	0.25	-4.44	0.13	3.23	0.22
$y = 0.2$							$y = 0.3$						
300	-12.78	0.06	-9.29	0.10	3.49	0.12	300	-11.97	0.21	-9.56	0.13	2.41	0.22
350	-11.16	0.06	-7.92	0.10	3.24	0.12	350	-10.45	0.10	-8.34	0.06	2.11	0.15
400	-10.03	0.12	-6.95	0.05	3.08	0.10	400	-9.45	0.20	-7.26	0.13	2.19	0.19
450	-9.17	0.09	-6.05	0.12	3.13	0.17	450	-8.15	0.10	-6.55	0.09	1.60	0.11
$y = 0.4$							$y = 0.5$						
300	-9.92	0.11	-5.47	0.13	4.45	0.18	300	-6.01	0.11	-1.46	0.09	4.55	0.05
350	-8.84	0.09	-4.33	0.07	4.14	0.03	350	-4.79	0.08	-0.44	0.07	4.36	0.12
400	-7.47	0.09	-2.80	0.05	4.67	0.11	400	-4.09	0.16	0.50	0.03	4.59	0.16
450	-6.65	0.12	-2.40	0.12	4.25	0.21	450	-3.43	0.14	1.24	0.04	4.67	0.16
$y = 0.6$							$y = 0.7$						
300	-3.65	0.13	0.09	0.15	3.74	0.19	300	-1.07	0.31	1.98	0.15	3.05	0.18
350	-2.46	0.18	1.35	0.10	3.80	0.14	350	0.15	0.26	3.04	0.08	2.88	0.23
400	-1.21	0.09	2.29	0.07	3.50	0.06	400	1.04	0.20	3.97	0.03	2.93	0.18
450	-0.47	0.08	2.69	0.12	3.16	0.18	450	2.14	0.11	4.78	0.05	2.64	0.15
$y = 0.8$							$y = 0.9$						
300	1.16	0.21	3.11	0.13	1.95	0.21	300	2.67	0.28	4.18	0.17	1.51	0.43
350	2.65	0.24	4.45	0.15	1.80	0.29	350	3.65	0.25	5.65	0.20	2.01	0.33
400	3.32	0.27	5.14	0.03	1.82	0.27	400	4.64	0.23	6.41	0.11	1.77	0.13
450	3.93	0.46	6.25	0.08	2.32	0.47	450	5.68	0.27	7.34	0.11	1.66	0.30
$y = 1$													
300	4.22	0.20	5.29	0.38	1.07	0.40							
350	5.21	0.19	6.66	0.12	1.45	0.27							
400	6.23	0.49	7.78	0.14	1.55	0.50							
450	7.18	0.31	8.58	0.12	1.40	0.26							

effects, which are a strong function of intermolecular forces between the solute molecules in the solution. Hence, solubility will highly depend on the thermodynamic stability of the solid phase as well as the molecular chain length in the solution. Similar effects have been seen in other binary alkane systems, notably the $C_{20}H_{42}$: $C_{22}H_{46}$ system [28].

The increase in T_e for the pure components $C_{16}H_{34}$ and $C_{18}H_{38}$ shows that the solubility of the solution decreased as the chain length increased, even though both components crystallised in the same structure, triclinic (T_p). The higher chain length increases the total van der Waals intermolecular interactions due to the increase in the number of $-CH_2$ chain groups, which increase the lattice energy [37]. Thus, more energy is required to break the lattice packing, decreasing the solubility and so increasing the saturation temperature. This result, not surprisingly, has been noted by a number of alkane solubility studies [23,28].

If the assumption was made that the solid structure of all the $C_{16}H_{34}$: $C_{18}H_{38}$ binary mixtures was triclinic, then, ideally, T_e could be determined by linear regression vs. composition (dashed lines in Fig. 3). The large decrease of T_e from the ideal line over $0.1 < y < 0.6$ of $C_{18}H_{38}$ is evidence of the presence of some more soluble phases with less stability than the hypothetical solid-solution. Whilst from $0.7 < y < 1.0$ of $C_{18}H_{38}$, T_e are very close to the ideal line with slightly lower values. This behaviour can be understood with respect to the ternary phase diagram of $C_{16}H_{34}$ / $C_{18}H_{38}$ /kerosene at a concentration of 308 g/l, as determined using in-situ synchrotron powder X-ray diffraction [34]. The resolved structures of the examined compositions are given at the bottom of Fig. 3. Hence, it will be clear to illustrate the trend of T_e vs. y , between $0.1 < y < 0.3$ of $C_{18}H_{38}$ the highly disordered rotator phase (R_1) is present, which causes the large decrease in T_e due to its low stability. After that, until composition of $C_{18}H_{38}$ reached $y = 0.5$, a higher stability crystalline orthorhombic phase (O_p) was observed corresponding to a higher T_e . Once $y = 0.7$ of $C_{18}H_3$ was in the mixture, the longer chain alkane component predominated the solid solution into the intrinsic

triclinic cell of $C_{18}H_{38}$. The decreased T_e seen for the mixtures in triclinic structure compared to the pure component triclinic structures is due to the difference in chain length, which increased lattice disorder and therefore decreased saturation temperature. The remaining region of $0.5 < y < 0.7$ of $C_{18}H_{38}$ has not as of yet been defined from the XRD studies. Within this region the T_e increases linearly with composition in $C_{18}H_{38}$, which could be either of the relatively less dense orthorhombic phase as $y = 0.5$ or higher density triclinic crystal structures as $y = 0.7$.

Overall, saturation temperatures reflect the higher stability of alkanes in the triclinic structure when compared to the binary mixture solid solutions in orthorhombic cells (R_1/O_p), as on heating the former dissolve at high temperatures. This is consistent with previous calculations of the crystal lattice energies, which show the triclinic phases to be more stable than the orthorhombic structures [38]. The close values of T_e from composition $y = 0.5$ (O_p) and 0.7 (T_p) of $C_{18}H_{38}$, suggests a decreased importance in terms of lattice stability between the triclinic and orthorhombic structures. This effect can be explained by the end group interactions of $-CH_3$ between the alkane chains becoming less significant as a function of increasing chain length as the interchain groups of $-CH_2$ attraction dominates.

4.2. Solution thermodynamics

4.2.1. Assessment of solubility and solution activity

According to Raoult's law, if the identical solid-form of the solute is crystallised in the solution as in the supercooled melt, (a_s) the activity of the solute in solution equals the activity of the solid phase (a). Furthermore, in an ideal solution the activity can be considered to be equal to the solution concentration (x_{ideal}), as given by Eq. (1):

$$a = a_s = x_{ideal} \quad (1)$$

In a non-ideal solution the activity can be determined through the

Table 4

Solubility (T_c) and supersolubility ($T_{c,l}$) data of $C_{16}H_{34}$: $C_{18}H_{38}$ mixtures in kerosene solvent, together with the calculated equilibrium MSZW (ΔT) over four concentrations (231–350 g/l). STD values from 5 recycles of repeats are also presented. y is the mole fraction of the longer alkane $C_{18}H_{38}$ in $C_{16}H_{34}$.

Con. (g/l)	$T_{c,l}$ (°C)	STD	T_c (°C)	STD	ΔT (°C)	STD	Con. (g/l)	$T_{c,l}$ (°C)	STD	T_c (°C)	STD	ΔT (°C)	STD
$y = 0$							$y = 0.1$						
231	-5.66	0.33	-3.35	0.08	2.30	0.30	231	-11.28	0.22	-6.24	0.10	5.04	0.22
269	-4.28	0.24	-1.85	0.07	2.44	0.23	269	-9.63	0.28	-4.57	0.10	5.06	0.30
308	-2.76	0.19	-0.50	0.09	2.26	0.24	308	-7.88	0.17	-3.34	0.07	4.54	0.16
350	-1.80	0.53	0.70	0.09	2.49	0.58	350	-7.00	0.18	-2.18	0.05	4.81	0.16
$y = 0.2$							$y = 0.3$						
231	-12.56	0.05	-8.48	0.07	4.08	0.11	231	-11.14	0.07	-9.29	0.10	1.85	0.15
269	-10.41	0.08	-6.44	0.06	3.97	0.14	269	-9.23	0.08	-7.68	0.14	1.56	0.21
308	-8.92	0.07	-4.90	0.06	4.02	0.11	308	-7.78	0.11	-6.10	0.14	1.68	0.21
350	-7.70	0.05	-4.12	0.04	3.58	0.04	350	-6.39	0.04	-5.19	0.09	1.20	0.12
$y = 0.4$							$y = 0.5$						
231	-9.44	0.03	-4.05	0.09	5.39	0.08	231	-5.85	0.14	-0.95	0.08	4.90	0.21
269	-7.59	0.09	-4.07	0.20	3.52	0.14	269	-4.46	0.08	0.52	0.03	4.98	0.07
308	-6.18	0.08	-2.24	0.23	3.94	0.20	308	-3.59	0.09	1.73	0.07	5.33	0.11
350	-4.89	0.08	-0.84	0.05	4.05	0.10	350	-2.59	0.05	2.92	0.05	5.52	0.04
$y = 0.6$							$y = 0.7$						
231	-3.08	0.21	1.17	0.09	4.24	0.27	231	-0.77	0.19	2.67	0.12	3.43	0.20
269	-1.55	0.23	2.73	0.12	4.28	0.28	269	0.61	0.12	4.05	0.09	3.44	0.20
308	-0.56	0.18	3.66	0.06	4.22	0.22	308	2.15	0.32	5.37	0.13	3.22	0.41
350	0.46	0.09	5.03	0.05	4.57	0.11	350	3.41	0.17	6.64	0.08	3.23	0.17
$y = 0.8$							$y = 0.9$						
231	1.26	0.54	4.07	0.09	2.81	0.47	231	3.56	0.22	5.56	0.14	2.00	0.36
269	3.43	0.14	5.59	0.08	2.17	0.15	269	5.43	0.18	7.20	0.08	1.77	0.22
308	4.24	0.19	6.88	0.09	2.64	0.24	308	6.70	0.23	8.29	0.03	1.59	0.25
350	5.62	0.40	8.14	0.03	2.52	0.41	350	7.71	0.24	9.56	0.08	1.85	0.18
$y = 1$													
231	5.06	0.21	6.85	0.13	1.79	0.29							
269	6.44	0.39	8.44	0.10	2.00	0.39							
308	7.89	0.27	9.47	0.06	1.58	0.26							
350	9.20	0.22	10.66	0.11	1.46	0.26							

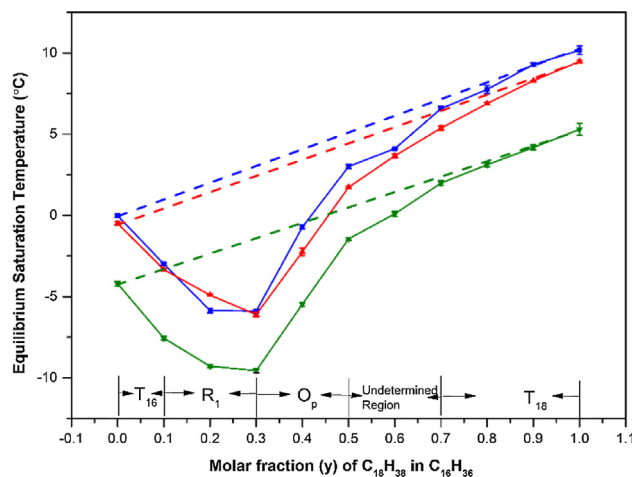


Fig. 3. Equilibrium saturation temperature (T_c) as a function of composition (y) for the $C_{16}H_{34}$: $C_{18}H_{38}$ binary mixtures in three solvents: (■) dodecane and (▲) kerosene at concentration of 308 g/l and (▼) toluene at 350 g/l. The dashed lines represent the linear regression of T_c based on the assessment of solid solution behaviour without any change in the underlying crystal structure, i.e. triclinic. Structural phases obtained from in-situ synchrotron X-ray diffraction analysis are also given with corresponding composition [34].

experimentally measured molar solubility (x) and the activity coefficient (γ), leading to the expression:

$$a = \gamma x \quad (2)$$

The activity coefficient (γ) of the solute in the saturated solution can

therefore be calculated using the relationships described by Eqs. (1) and (2), thus:

$$\gamma = \frac{x_{ideal}}{x} \quad (3)$$

The concept of an ideal solution is predicated on the assumption that for a given solute in an ideal solution, the interaction of solute molecules with other solute molecules is the same as with solvent molecules. Under this assumption and that the contribution of heat capacity C_p is negligible over the range of temperatures used, which is a common simplification used that introduces only a very minor error [39,40], the ideal solid-liquid equilibrium model can be expressed through the van't Hoff equation (Eq. (4)):

$$\ln(x) = \frac{\Delta H_f}{R} \left[\frac{1}{T} - \frac{1}{T_m} \right] \quad (4)$$

where the melting point (T_m) and the corresponding enthalpy of fusion (ΔH_f) of the 11 different compositions for the $C_{16}H_{34}$: $C_{18}H_{38}$ mixtures solute were obtained from DSC measurements [34].

At the melting point (T_m), the enthalpy of fusion (ΔH_f) can be related to the entropy of fusion (ΔS_f) by Eq. (5):

$$\Delta S_f = \frac{\Delta H_f}{T_m} \quad (5)$$

Therefore, Eq. (4) can be rewritten as:

$$\ln(x) = -\frac{\Delta H_f}{RT} + \frac{\Delta S_f}{R} \quad (6)$$

In a non-ideal solution the deviation from ideality can be accounted for by modification of the right hand side of the van't Hoff expression, allowing the solubility to be written as:

$$\ln(x) = -\frac{\Delta H_{diss}}{RT} + \frac{\Delta S_{diss}}{R} \quad (7)$$

Where ΔH_{diss} and ΔS_{diss} are the enthalpy and entropy of dissolution, respectively.

Using this expression, by plotting $\ln(x)$ versus $1/T$, the temperature dependence molar solubility of a “single solute” (experimental data) is described by an enthalpic term obtained from the slope ($-\frac{\Delta H_{diss}}{R}$), referred to as the van't Hoff enthalpy of solution. All thermodynamic data is referenced to standard state conditions.

The calculated activity coefficients were fitted with respect to the variation in temperature, by:

$$\ln(\gamma) = mT + c \quad (8)$$

where m and c are constants.

4.2.2. Solution thermodynamics analysis

van't Hoff analysis provides further indication of the solution behaviour in terms of solvent and compositional effects. The van't Hoff plots fit well by linear regression for all solutions studied. This indicates a consistent heat of fusion as a function of solution concentration, corroborating that the solid-state form of the crystallising solute was the same within the corresponding range of temperature. Example plots for selected $C_{16}H_{34}:C_{18}H_{38}$ mixtures in three solvents are shown in Fig. 4. The enthalpy (ΔH_{diss}) and entropy (ΔS_{diss}) of dissolution values calculated from van't Hoff analysis are summarised in Table 5.

The results from Fig. 4 indicate that non-ideal behaviour was observed for all the three solvents, but the solutions showing behaviour most closely to an ideal solution were those in dodecane solvent,

followed by kerosene and then toluene. This is due to the non-polar alkane mixtures, which are more soluble in an alkane, non-polar solvent, and so the binary mixtures have the highest solubility in dodecane. Kerosene is a mixture of alkane and aromatic components; therefore it shows the next highest solubility. Due to toluene being aromatic in nature the alkane mixtures are least soluble in this solvent environment. The ideality plots also show that the pure component solutions are closer to ideal solutions than the binary equimolar mixture, as the solution plots are much closer to the ideal plots for the pure component solutions.

It should be noted that an increased solubility in kerosene and dodecane solutions follows a decline in the slope of the curve and hence a reduction in van't Hoff enthalpy of dissolution (ΔH_{diss}). This behaviour was observed in most of the compositions as seen in Table 5, however, exceptions are observed in $y = 0.3$ of $C_{18}H_{38}$ with higher ΔH_{diss} in dodecane as compared with kerosene and toluene. The enthalpy of dissolution differences occur between the solute-solute (solid-state) and solute-solvent (solvation) intermolecular interaction energies. If we assume that all crystal structures formed are independent of the solvent used then the lowest solubility system would require the highest solvation energy and as such, the highest dissolution energy. For the three solvents used, toluene would show the highest dissolution enthalpy, whereas dodecane would show the lowest dissolution enthalpy, as shown in Table 5. Thus, the abnormal behaviour of $y = 0.3$ of $C_{18}H_{38}$ in dodecane with high ΔH_{diss} can be related to different phase formation occurring in comparison to the other solvents at this composition; this is also seen with a steeper slope of solubility plot for this solution (Fig. 4b). Apart from this abnormal point in Table 5, ΔH_{diss} and ΔS_{diss}

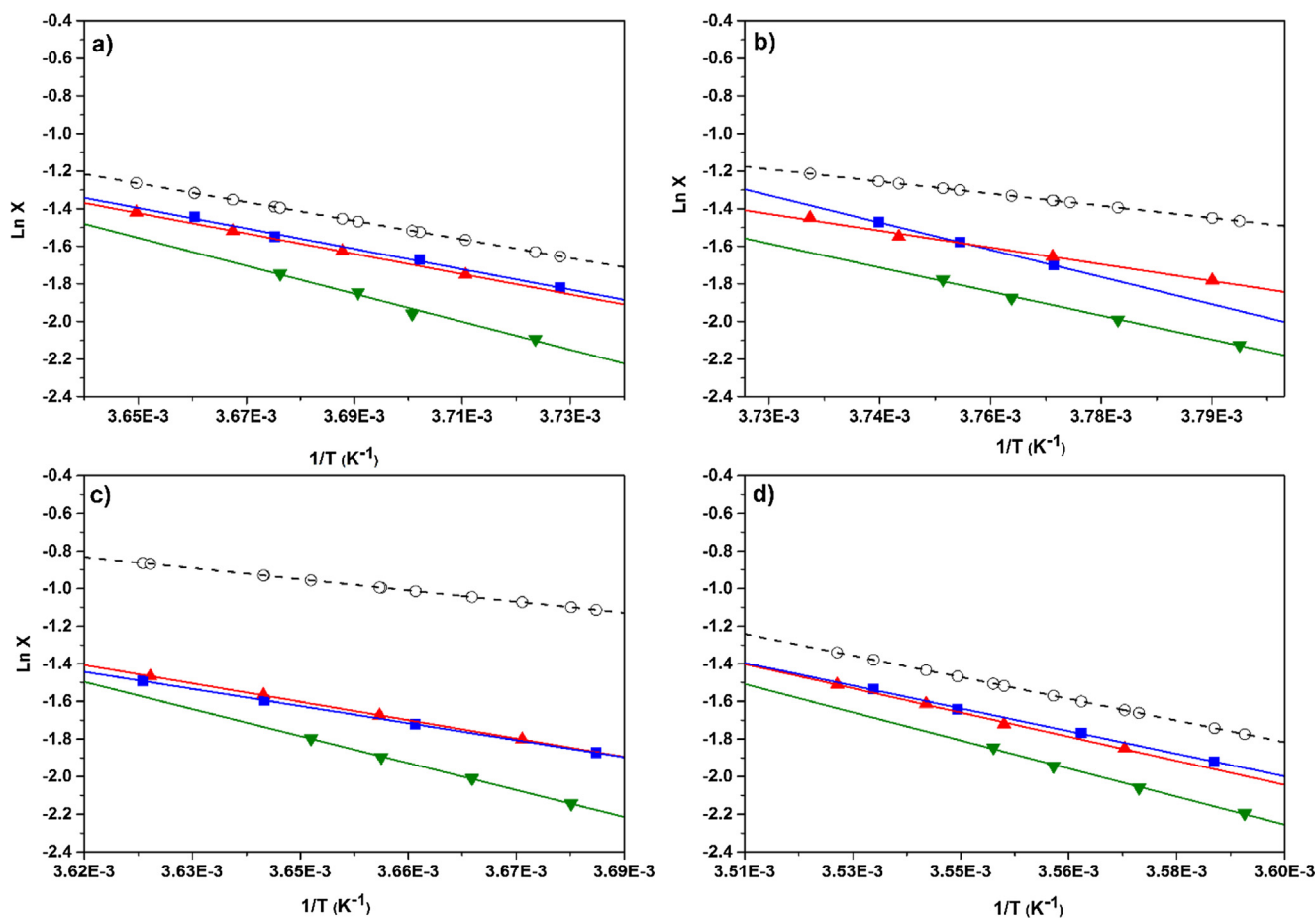


Fig. 4. van't Hoff ideality plots for $C_{16}H_{34}:C_{18}H_{38}$ binary mixtures in three solvents: dodecane, toluene and kerosene. (a) Pure $C_{16}H_{34}$. (b) $y = 0.3$ of $C_{18}H_{38}$. (c) $y = 0.5$ of $C_{18}H_{38}$. (d) Pure $C_{18}H_{38}$. Symbols (○) Ideal, (■) Dodecane, (▲) Kerosene, (▼) Toluene.

Table 5

Thermodynamic parameters derived from the poly-thermal method solubility data for all compositions of the $C_{16}H_{34}:C_{18}H_{38}$ mixtures in dodecane, toluene and kerosene solvents.

$y: C_{18}H_{38}$	ΔH_{diss} (kJ mol ⁻¹)			ΔS_{diss} (kJ mol ⁻¹ K ⁻¹)			ΔH_{fus} (kJ mol ⁻¹)	T_m (°C)	γ		
	Dodecane	Kerosene	Toluene	Dodecane	Kerosene	Toluene			Dodecane	Kerosene	Toluene
0	50.12	49.9	68.66	0.17	0.17	0.24	45.78	19.05	1.18–1.14	1.20–1.17	1.59–1.42
0.1	45.97	49.17	63.75	0.16	0.17	0.22	32.13	16.79	1.81–1.61	1.84–1.64	2.41–2.02
0.2	52.65	43.43	62.91	0.18	0.15	0.22	34.63	17.35	1.53–1.24	1.45–1.34	1.94–1.66
0.3	75.21	46.34	66.34	0.27	0.16	0.23	33.60	18.26	1.63–1.24	1.39–1.26	1.93–1.62
0.4	54.64	51.91	62.72	0.19	0.18	0.22	33.70	19.47	1.81–1.57	1.79–1.53	2.32–1.95
0.5	50.26	54.00	79.62	0.17	0.18	0.28	32.97	20.67	2.14–1.87	2.07–1.82	2.84–2.32
0.6	51.01	56.02	80.41	0.17	0.19	0.28	34.13	21.99	2.08–1.82	2.13–1.87	2.83–2.30
0.7	49.38	54.02	79.12	0.16	0.18	0.27	35.34	23.36	2.13–1.91	2.10–1.87	2.86–2.36
0.8	49.99	53.73	73.21	0.17	0.18	0.25	44.36	24.69	1.61–1.55	1.64–1.55	2.17–1.90
0.9	50.74	55.85	72.53	0.17	0.19	0.24	48.21	26.76	1.41–1.39	1.44–1.38	1.84–1.64
1	55.68	59.29	69.06	0.18	0.20	0.23	53.11	28.6	1.20–1.17	1.22–1.19	1.52–1.40

ΔH_{fus} obtained from previous DSC analysis [34]. All data is referenced to standard state.

were highest in the mixture sample with $y = 0.6 C_{18}H_{38}$ in all three solvents, which indicates a phase transition might occur at this point. Correlating to the T_e trend observation, it could be illustrated by the transition from Op to Triclinic at $y = 0.6 C_{18}H_{38}$.

Activity coefficients (γ) were calculated for each composition of the $C_{16}H_{34}:C_{18}H_{38}$ binary mixtures in all three solvents over the range of concentrations used. All values are greater than one, see Table 5, showing that the solutions had less than ideal behaviour, suggesting that association of alkane molecules was more favoured in these solutions [41]. Fig. 5 reveals a consistent trend in the activity coefficients as a function of composition for all three solvents, with the highest deviation being observed in toluene due to the lower solubility. For all three solvents, the highest activity coefficients are seen for the possible orthorhombic and triclinic structures, between the region of $0.5 < y < 0.7 C_{18}H_{38}$ binary mixture. This behaviour indicates that the large deviation from ideality is not solvent dependent but reflects differences in the crystal structure of the precipitated phase. Notably, the experimental solubility is much lower in this as of yet undefined structural region than the R_1 phase, perhaps related to the higher stability of the more ordered phases (O_p/T_p) forming in the adjacent regions of the phase diagram.

4.3. Assessment of crystallisability

The assessment of crystallisability, giving an indication as to the extent a solution can be undercooled, was carried out from the calculation of equilibrium Meta-stable zone width (MSZW), by the expression:

$$MSZW = T_e - T_{c,l} \quad (9)$$

Variations in the crystallisability of the solutions, as assessed from the MSZWs, as a function of composition were observed, (Fig. 6). The trends in these were found to be analogous to those found in the solubility data with a strong correlation to the known solid-state structures. For example, relatively lower values of MSZW were present for the solutions containing the pure single components as well as for the binary mixtures ranging from $y = 0.8$ to 1 of $C_{18}H_{38}$, where solid-solution behaviour within the triclinic phase region might be anticipated.

Maxima in the observed MSZWs were observed for the $y = 0.1$ and 0.5 of $C_{18}H_{38}$ in the binary mixture for all three solutions. In this region the effect at $y = 0.1$ is consistent with the smaller quantity of the longer $C_{18}H_{38}$ molecules disrupting the crystallisation of $C_{16}H_{34}$ within the triclinic phase, where the shorter c-axis of the latter cannot easily accommodate the longer $C_{18}H_{38}$ molecule without chain folding [42]. As shown in Fig. 6, these maxima correspond to the phase transition points between $T_{16} - R_1$ and $O_p - T_{18}$ regions, respectively. As these two mixtures had relatively low saturation temperatures, the resultant

greater MSZW could be explained by the relatively lower temperature of crystallisation corresponding to a larger nucleation barrier.

A number of conclusions can be drawn from this data. Firstly, the crystallisability as a function of solvent is mostly equivalent for the 3 solvents studied with dodecane solutions, in general, crystallising easier than toluene and kerosene solutions. There are two regions where this appears not to be the case. At the higher $C_{16}H_{34}$ ($y = 0.1$) content and also where the $C_{16}H_{34}$ and $C_{18}H_{38}$ are roughly equimolar ($0.4 < y < 0.5$). In both cases this effect probably reflects a combination of the high solubility for these compositions and the inhibition of $C_{16}H_{34}$ crystallisation by the longer $C_{18}H_{38}$ homologue. Also, at $y = 0.1$ the closeness in chain length between solute and solvent ($C_{12}H_{26}$) may cause solvent inhibition of the crystallisation process due to solid-solution formation.

Also, the crystallisability is higher towards the higher $C_{18}H_{38}$ content. Here the $C_{18}H_{38}$ lattice can more easily accommodate the shorter $C_{16}H_{34}$ chain length in contrast to the $C_{16}H_{34}$ higher content end of the binary mixture where the longer chain length can only be incorporated by incipient chain folding of the longer homologue [42]. An exception to this general trend seems to occur in the region of the phase diagram where the less stable rotator phase results from crystallisation. This, in turn, appears to crystallise, not surprisingly, much more easily than in the region where the much more stable triclinic phase is formed.

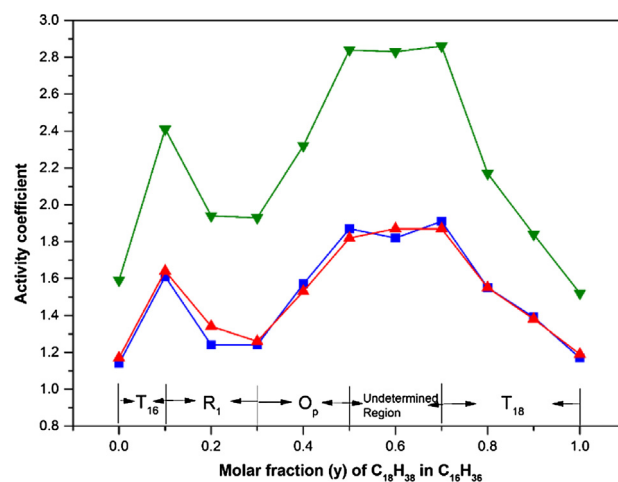


Fig. 5. Activity coefficient (γ) as a function of composition for the $C_{16}H_{34}:C_{18}H_{38}$ binary mixtures in three solvents: (■) dodecane and (▲) kerosene at a concentration of 308 g/l and (▼) toluene at 350 g/l. Structural phases obtained from the in-situ synchrotron X-ray diffraction analysis are given with the corresponding composition [34].

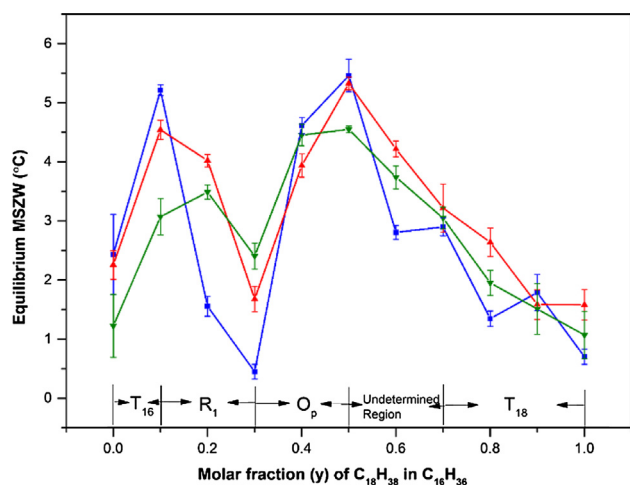


Fig. 6. Equilibrium MSZW patterns as a function of composition for $C_{16}H_{34}:C_{18}H_{38}$ binary mixtures in three solvents: (■) dodecane and (▲) kerosene at a concentration of 308 g/l and (▼) toluene at 350 g/l. Structural phases obtained from the in-situ synchrotron X-ray diffraction analysis are given with the corresponding composition [34].

5. Conclusions

This work has reported the solubility and metastability of $C_{16}H_{34}:C_{18}H_{38}$ binary mixtures in three solvents, dodecane, toluene and kerosene, as measured using poly-thermal analysis, as a function of composition, solution concentration and cooling rate.

Equilibrium saturation temperature analysis suggests that structural behaviour of the alkane solutions is independent of the solvents and concentrations used in this study. Also, as the carbon length of alkanes is increased, the solubility decreases due to an increased van der Waals interaction. Furthermore, less stable crystal structures form from the binary mixtures when compared to the single component solutes $C_{16}H_{34}$ and $C_{18}H_{38}$. These structures were found to be consistent with the rotator (R_1), orthorhombic (O_p) and triclinic (T_p) phase regions. These structural changes provide the significant decrease in T_c values observed in the solutions containing $C_{16}H_{34}:C_{18}H_{38}$ binary mixtures. This conclusion is further indicated by the van't Hoff analysis with ΔH_{diss} and ΔS_{diss} being found to follow the trend dodecane < kerosene < toluene.

Although non-ideal behaviour was observed for all solutions within $C_{16}H_{34}:C_{18}H_{38}$ binary mixtures, the solubility is found to be in good agreement with activity coefficients with higher solubility in dodecane and the closest to the ideal condition, followed by kerosene and toluene. Furthermore, the activity coefficient is found to reflect the non-identical phase formation in solution crystallisation as the high deviation value was observed from $C_{18}H_{38}$ molar composition of $0.5 < y < 0.7$ in all three solvents.

Measurement of crystallisability as a function of solute composition and solvent were found to mirror the solubility data as evidenced by a high dependency of the measured MSZWs on the known solid form formation behaviour, the composition and solution effects.

Overall, a comprehensive study of the solubility of HVO blended diesel fuel representative solutions was completed, with fundamental knowledge on solution saturation temperature, MSZW and activity being obtained. Along with the corresponding paper relating towards the nucleation kinetics of these solutions, a foundation for the improvement of HVO blended diesel fuel cold flow behaviour has been built.

Notes

The authors declare no competing financial interest.

Acknowledgements

The authors gratefully acknowledge Infineum Ltd. for the funding of this research, which forms part of the doctoral studies of one of us (X. Tang). We also gratefully acknowledge the U.K. EPSRC for their support of nucleation and crystal growth research at Leeds and Manchester through funding the Critical Mass Project: Molecules, Clusters and Crystals (Grant references EP/IO14446/1 and EP/IO13563/1).

References

- [1] Sorda G, Banse M, Kemfert C. An overview of biofuel policies across the world. *Energy Policy* 2010;38(11):6977–88.
- [2] Aatola H, Larmi M, Sarjovaara T, Mikkonen S. Hydrotreated Vegetable Oil (HVO) as a renewable diesel fuel: trade-off between NOx, particulate emission, and fuel consumption of a heavy duty engine. *SAE Int J Engines* 2008;1(1):1251–62.
- [3] Liu Y, Sotelo-Boyas R, Murata K, Minowa T, Sakanishi K. Hydrotreatment of vegetable oils to produce bio-hydrogenated diesel and liquefied petroleum gas fuel over catalysts containing sulfided Ni–Mo and solid acids. *Energy Fuels* 2011;25(10):4675–85.
- [4] Bacha J, Freel J, Gibbs A, Gibbs L, Hemighaus G, Hoekman K, Horn J, Gibbs A, Ingham, M, Jossens L. Diesel fuels technical review. *Chevron Global Marketing* 2007.
- [5] Muller A. A further X-ray investigation of long chain compounds (n-Hydrocarbon). *Proc Roy Soc London A* 1928;120(785):437–59.
- [6] Muller A. The crystal structure of the normal paraffins at temperatures ranging from that of liquid air to the melting points. *Proc Royal Soc London A* 1930;127(805):417–30.
- [7] Müller A. An X-ray investigation of normal paraffins near their melting points. *Proc Royal Soc London A* 1932;138(836):514–30.
- [8] Müller A, Lonsdale K. The low-temperature form of $C_{18}H_{38}$. *Acta Crystallogr A* 1948;1(3):129–31.
- [9] Smith A. The crystal structure of the normal paraffin hydrocarbons. *J Chem Phys* 1953;21(12):2229–31.
- [10] Shearer H, Vand V. The crystal structure of the monoclinic form of n-hexatriacontane. *Acta Crystallogr A* 1956;9(4):379–84.
- [11] Nyburg S, Lüth H. N-Octadecane: a correction and refinement of the structure given by Hayashida. *Acta Crystallogr B: Struct Crystallogr Crystal Chem* 1972;28(10):2992–5.
- [12] Retief J, Engel D, Boonstra E. X-ray powder diffractometric procedure for lattice parameter determination for long-chain molecules. *J Appl Crystallogr* 1985;18(3):150–5.
- [13] Retief J, Engel D, Boonstra E. Lattice parameters of solid solutions of long-chain n-alkanes. *J Appl Crystallogr* 1985;18(3):156–8.
- [14] Nyburg S, Potworowski J. Prediction of unit cells and atomic coordinates for the n-alkanes. *Acta Crystal B: Struct Crystallogr Cryst Chem* 1973;29(2):347–52.
- [15] Lüth H, Nyburg S, Robinson P, Scott H. Crystallographic and calorimetric phase studies of the n-eicosane, $C_{20}H_{42}$: n-docosane, $C_{22}H_{46}$ system. *Mol Cryst Liq Cryst* 1974;27(3–4):337–57.
- [16] Craig SR, Hastie GP, Roberts KJ, Sherwood JN. Investigation into the structures of some normal alkanes within the homologous series $C_{13}H_{28}$ to $C_{60}H_{122}$ using high-resolution synchrotron X-ray powder diffraction. *J Mater Chem* 1994;4(6):977–81.
- [17] Denicolò I, Doucet J, Craievich AF. X-ray study of the rotator phase of paraffins (III): even-numbered paraffins $C_{18}H_{38}$, $C_{20}H_{42}$, $C_{22}H_{46}$, $C_{24}H_{50}$, and $C_{26}H_{54}$. *J Chem Phys* 1983;78(3):1465–9.
- [18] Doucet J, Denicolò I, Craievich AF, Germain C. X-ray study of the rotator phase of paraffins (IV): $C_{27}H_{56}$, $C_{28}H_{58}$, $C_{29}H_{60}$, $C_{30}H_{62}$, $C_{32}H_{66}$, and $C_{34}H_{70}$. *J Chem Phys* 1984;80(4):1647–51.
- [19] Ungar G, Masic N. Order in the rotator phase of n-alkanes. *J Phys Chem* 1985;89(6):1036–42.
- [20] Sirota EB, Herhold AB. Transient rotator phase induced nucleation in n-alkane melts. *Polymer* 2000;41(25):8781–9.
- [21] Mondieig D, Rajabalee F, Metivaud V, Oonk HAJ, Cuevas-Diarte MA. N-alkane binary molecular alloys. *Chem Mater* 2004;16(5):786–98.
- [22] Coutinho JAP, Andersen SI, Stenby EH. Evaluation of activity coefficient models in prediction of alkane solid-liquid equilibria. *Fluid Phase Equilib* 1995;103(1):23–39.
- [23] Provost E, Chevallier V, Bouroukba M, Petitjean D, Dirand M. Solubility of some n-alkanes (C_{23} , C_{25} , C_{26} , C_{28}) in heptane, methylcyclohexane, and toluene. *J Chem Eng Data* 1998;43(5):745–9.
- [24] Ghogomu PM, Dellacherie J, Balesdent D. Solubility of normal paraffin hydrocarbons (C_{20} to C_{24}) and some of their binary mixtures ($C_{22} + C_{24}$) and ($C_{23} + C_{24}$) in ethylbenzene. *J Chem Thermodyn* 1989;21(9):925–34.
- [25] Chang SS, Maurey JR, Pummer WJ. Solubilities of two n-alkanes in various solvents. *J Chem Eng Data* 1983;28(2):187–9.
- [26] Domańska U, Rolińska J. Correlation of the solubility of even-numbered paraffins $C_{20}H_{42}$, $C_{24}H_{50}$, $C_{26}H_{54}$, $C_{28}H_{58}$ in pure hydrocarbons. *Fluid Phase Equilib* 1989;45(1):25–38.
- [27] Domańska U. Solubility of n-paraffin hydrocarbons in binary solvent mixtures. *Fluid Phase Equilib* 1987;35(1):217–36.
- [28] Gerson AR, Roberts K, Sherwood J, Taggart A, Jackson G. The role of growth environment on the crystallization of normal alkanes in the homologous series from

- C18H38 to C29H60. *J Cryst Growth* 1993;128(1–4):1176–81.
- [29] Flöter E, Hollanders B, de Loos TW, de Swaan Arons J. The ternary system (n-Heptane + Docosane + Tetracosane): the solubility of mixtures of docosane and tetracosane in heptane and data on solid–liquid and solid–solid equilibria in the binary subsystem (Docosane + Tetracosane). *J Chem Eng Data* 1997;42(3):562–5.
- [30] Cunningham DAH, Gerson AR, Roberts KJ, Sherwood JN, Wojciechowski K. Quantifying some of the structural aspects of crystallization processes: experiments using synchrotron radiation. In: Garside J, Davey RJ, Jones AG, editors. *Advances in industrial crystallization*. London: Butterworths; 1991. p. 101–30.
- [31] Gerson AR, Roberts KJ, Sherwood JN, Cernik R, Pattison P, Fitch A. *Synchrotron light: applications and related instrumentation 2*. Singapore: World Scientific; 1990.
- [32] Gerson AR. *Structural and kinetic aspects of the crystallisation of n-alkanes, homologues, mixtures and real waxes*. University of Strathclyde; 1990.
- [33] Gerson AR, Roberts KJ, Sherwood JN. X-ray powder diffraction studies of alkanes: unit-cell parameters of the homologous series C18H38 to C28H58. *Acta Crystallograph B: Struct Sci Cryst Eng Mater* 1991;B47:280–4.
- [34] Tang X. *Crystal Structure, Phase Behaviour and Kinetics Associated with the Crystallisation of Octadecane, Hexadecane, and Mixtures Thereof*, University of Leeds 2017.
- [35] Tang X, Kaskiewicz PL, Camacho Corzo DM, Lai X, Roberts KJ, Dowding P, More I. Data for crystallisation, dissolution and saturation temperatures of the ternary system: hexadecane and octadecane representative in fuel solvents. Data in Brief In press.
- [36] Technobis Crystal 16. <https://www.crystallizationsystems.com/crystal16>.
- [37] Clydesdale G, Roberts KJ. Structural stability and morphology of even number n-alkanes crystallising in the homologous series C18H38–C28H58. 1991; 87:130–137.
- [38] Taggart A, Voogt F, Clydesdale G, Roberts K. An examination of the nucleation kinetics of n-alkanes in the homologous series C13H28 to C32H66, and their relationship to structural type, associated with crystallization from stagnant melts. *Langmuir* 1996;12(23):5722–8.
- [39] Turner TD, Corzo DMC, Toroz D, Curtis A, Dos Santos MM, Hammond RB, et al. The influence of solution environment on the nucleation kinetics and crystallisability of para-aminobenzoic acid. *PCCP* 2016;18(39):27507–20.
- [40] Prausnitz JM, Lichtenthaler RN, Gomes de Azevedo E. *Molecular thermodynamics of fluid-phase equilibria*. third ed. New Jersey: Prentice Hall PTR; 1999.
- [41] Camacho Corzo DM. *Crystallisation in Diesel and Biodiesel Fuel in Relation to their Solution Composition*. University of Leeds, 2015.
- [42] Hastie GP, Roberts KJ. Investigation of inter- and intra-molecular packing in the solid state for crystals of normal alkanes and homologous mixtures using FT-IR spectroscopy. *J Mater Sci* 1994;29(7):1915–9.